Stem Cell Research & Therapy

RESEARCH

Open Access

Impact of photobiomodulation on neural embryoid body formation from immortalized adipose-derived stem cells

Precious Earldom Mulaudzi[1], Heidi Abrahamse[1] and Anine Crous[1*]

Abstract

Background Embryoid bodies (EBs) are three-dimensional (3D) multicellular cell aggregates that are derived from stem cell and play a pivotal role in regenerative medicine. They recapitulate many crucial aspects of the early stages of embryonic development and is the first step in the generation of various types of stem cells, including neuronal stem cells. Current methodologies for differentiating stem cells into neural embryoid bodies (NEBs) in vitro have advanced significantly, but they still have limitations which necessitate improvement. Photobiomodulation (PBM) a low powered light therapy is a non-invasive technique shown to promote stem cell proliferation and differentiation.

Methods This in vitro study elucidated the effects of photobiomodulation (PBM) on the differentiation of immortalized adipose-derived stem cells (iADSCs) into NEBs within a 3D cell culture environment. The study utilized PBM at wavelengths of 825 nm, 525 nm, and a combination of both, with fluences of 5 and 10 J/cm^2. Morphology, viability, metabolic activity, and differentiation following PBM treatment was analysed.

Results The results revealed that the effects of photobiomodulation (PBM) are dose dependent. PBM, at 825 nm with a fluence of 10 J/cm^2, significantly enhanced the size of neural embryoid bodies (NEBs), improved cell viability and proliferation, and reduced lactate dehydrogenase (LDH) levels, indicating minimal cell damage. Interestingly, the stem cell marker CD 44 was upregulated at 5 J/cm^2 in all treatment groups at 24 and 96 hpi, CD105 increased with 825 nm at 10 J/cm^2 at 24 hpi, which may be attributed to a heterogeneous cell population within the NEBs. Pax6 expression showed transient activation. Nestin was upregulated at 825 nm with 10 J/cm^2 at 96 hpi, suggesting a promotion of neural precursor populations. GFAP an intermediate filament protein was upregulated at 825 nm at 10 J/cm2 at both 24 and 96 hpi. SOX2, a pluripotency marker, was expressed at 5 J/cm^2 across all wavelengths. Neu N a neuronal nuclei marker was expressed at 5 J/cm^2 in all treatments at 24 hpi and over time the expression was observed in all treatment groups at 10 J/cm^2.

Conclusion In conclusion, the application of PBM at 825 nm with a fluence of 10 J/cm^2 during the differentiation of iADSCs into NEBs resulted in optimal differentiation. Notably, the neuronal marker Nestin was significantly upregulated, highlighting the potential of the PBM approach for enhancing neuronal differentiation its promising applications in regenerative medicine.

Keywords Photobiomodulation, Cell differentiation, Stem cells, Neural embryoid body

*Correspondence:
Anine Crous
acrous@uj.ac.za

Graphical Abstract

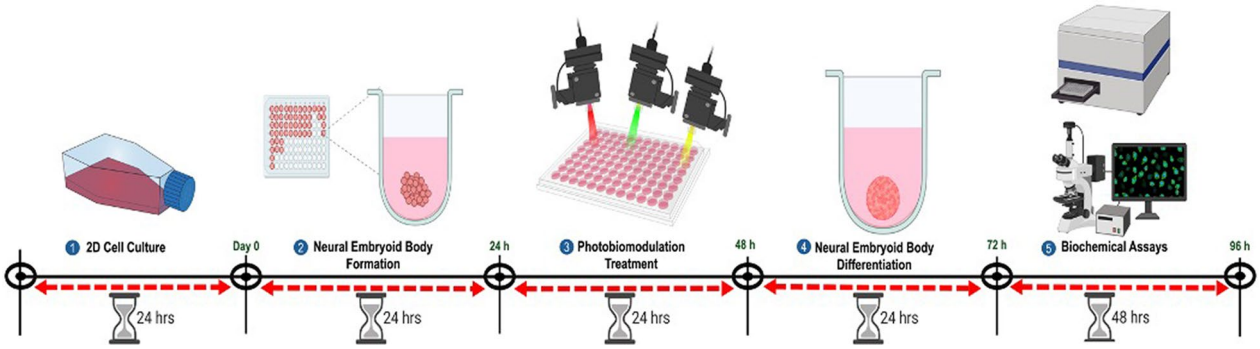

Introduction

The field of stem cell research has changed the fundamental notions about regenerative medicine and tissue engineering. Stem cells hold great promise in the treatment of a wide range of diseases and injuries because of their unique capacity to self-renew and differentiate into various cell types [1]. Adipose-derived stem cells (ADSCs) have been recognized as highly suitable candidates in regenerative medicine due to their capacity to undergo cellular differentiation into various cell lineages including neuronal cells through manipulation [2, 3]. Compared to mesenchymal stem cells from bone marrow, for in vitro studies ADSCs have a higher proliferation rate, differentiation capability, and the least amount of apoptosis [2]. Immortalized adipose-derived stem cells (iADSCs) have shown to be of high interest in regenerative therapy because of their abundance, ability to maintain properties of parent cells and differentiation ability [4]. Furthermore, stem cell source can have significant ethical implications, where ADSCs offer a more compelling alternative to bone marrow-derived stem cells (BMDSCs) due to their less invasive and more ethically favourable collection process [5].

Various methods have been employed to induce the transformation of iADSCs into neuronal cells for clinical applications. The application of low-level laser therapy, also known as photobiomodulation (PBM) [6]. PBM has been observed to elicit many effects, including the augmentation of intracellular activities, promotion of cell proliferation, and facilitation of stem cell differentiation [7, 8]. Specific wavelength of laser light and duration of exposure are critical factors that influence the regulatory effects of PBM on cellular activity [9]. Specific wavelengths of light, when applied to stem cell cultures, may enhance neural marker expression and encourage the development of neural progenitors [2, 10]. Stem cell activity and gene expression alterations, brought on by PBM, have the potential to enhance cell differentiation and proliferation [7, 10].

Recent research has increasingly focused on applying PBM to enhance neural cell development from ADSCs. However, most of this work has been conducted in two-dimensional cultures [2, 11]. To bridge the gap between in vitro and in vivo cell culture, this study innovatively utilizes multiple or combined wavelengths of PBM and advances the research by employing a three-dimensional (3D) culture system, which more accurately mimics the in vivo environment. Several techniques are currently being studied and validated for the transdifferentiation of ADSCs into neurons, aiming to advance potential therapeutic applications in regenerative medicine [12, 13]. Advances in cell culture has shifted from working within a monolayer cell culture to three-dimensional (3D) cell culture. This is mainly because cells in 3D show more complex cell-to-cell interaction, and are grown in aggregates [14]. In a 3D cell culture environment, cells are differentiated into neural embryoid bodies. Neural embryoid bodies (NEBs) are 3D neural cell aggregates from pluripotent stem cells, mimicking early neural development stages, providing valuable models for studying neurogenesis, differentiation, and tissue formation [15].

The effects of PBM vary based on laser light exposure, cell type, and physiological context. Therefore, this study aims to explore the effects of PBM at 825 nm (NIR) and 525 nm (green) and a combination of both at low (5 J/cm^2) and high dose (10 J/cm^2) in a 3D cell culture environment in the transdifferentiation of ADSCs into NEBs. Herein, we explore the effects of PBM on the transdifferentaiation of iADSCs into NEBs. Biochemical changes in NEB structure and morphological changes were also evaluated. Finally, gene expression of early neural

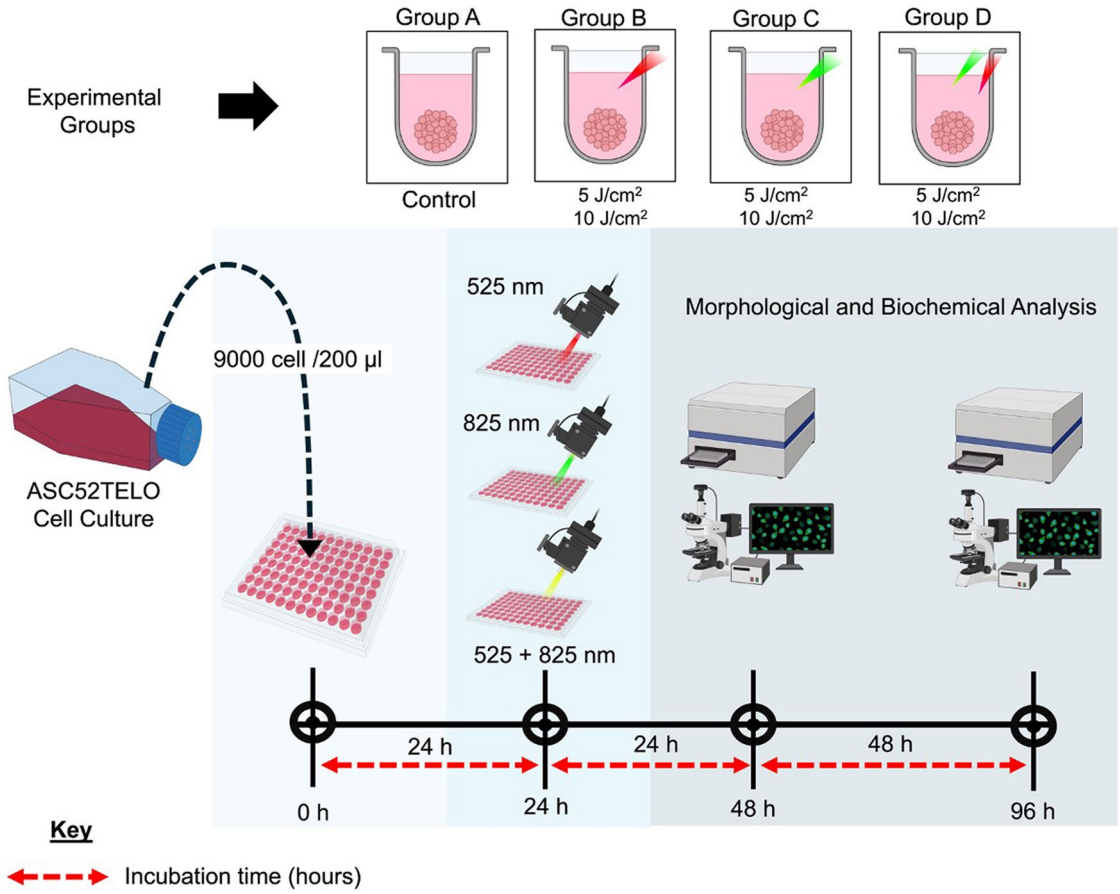

Fig. 1 Methodology overview

markers and ADSCs markers were investigated to understand the effect of PBM in gene expression levels.

Materials and methods

Experimental model

This experiment was divided into 4 groups (Fig. 1): There were three experimental groups and one control group (Group A) both of which cells were grown in EB formation media. Experimental groups received different PBM treatment, Group B (Experimental 1) PBM treatment at 825 nm, Group C (Experimental 2) PBM treatment 525 nm, Group D (Experimental 3) PBM treatment at 525 and 825 nm. The experimental cell culture model has been represented in depicting fluences of 5 and 10 J/cm^2.

Cell Culture

ADSCs Cell culture

Immortalised ADMSCs (ASC52telo hTERT, ATCC SCRC-4000™) from American Type Culture Collection (ATCC) was used in this study. Dulbecco's Modified Eagle Media (DMEM) (Sigma- Aldrich, South Africa) supplemented with 20% fetal bovine serum (FBS Superior) (Biochrom, South Africa) and 1% antibiotics: 0.5% Penicillin–Streptomycin (Sigma-Aldrich, South Africa) and 0.5% Amphotericin B solution (Sigma-Aldrich, South Africa). Cultured cells were maintained and incubated at 37 °C in 5% CO_2 and 85% humidity incubator till confluency of 80–90%. Upon confluency complete media was discarded and cells were washed twice with Hank's balanced salt solution (HBSS). Experimental cells were detached from the culture flask with TrypLE (Invitrogen, 12,605–028). Afterwards, the experimental cells were cultured in a U bottom ultra-low attachment 96 well plate (Corning, CLS4520) at a concentration of 450 cells /µL.

Neural Embryoid Body (NEB) Formation and differentiation

Neural embryoid bodies (NEBs) were formed using modified low attachment surface technique. Neural embryoid bodies were produced by seeding 9000 cells in 200µL of embryoid body (EB) formation media. The EB formation medium consisted of DMEM, supplemented with 20% fetal bovine serum, 1% antibiotics: 0.5% Penicillin–Streptomycin and 0.5% Amphotericin B solution, 4 ng/mL

basic fibroblast growth factor (Sigma, South Africa) and 5 µM ROCK inhibitor (Sigma, South Africa). The well plate was centrifuged at 3000 gravitational forces (xg) for 5 min to allow cells to aggregate and incubated and maintained in static culture conditions for 24 h to enable NEB compaction prior to photobiomodulation treatment.

Photobiomodulation

After 24 h of incubation, the embryoid formation media was changed prior to irradiation, cells were irradiated with G 825 nm Diode Laser (National Laser Centre of South Africa, SN 070900108), NIR 525 nm Diode Laser (National Laser Centre of South Africa, EN 60825–1:2007) and G-NIR (525 and 825 nm) combination wavelengths at fluences of 5 and 10 J/cm^2. The power of the laser output (mW) was measured using a FieldMate Laser Power Meter, a High-Sensitivity Thermopile Sensor PM3 (Coherent, South Africa, 1,098,336) was used to determine the irradiation time of the laser based on fluency. The laser parameters used in the present study are displayed in Table 1.

Morphology

Cellular morphological changes were analyzed using inverted light microscope (Wirsan, Olympus CKX41) with attached microscope-connected digital camera (Olympus, SC30) at 24 and 96 h post irradiation (hpi). NEB size was determined by measuring the diameter of NEBs with 2 arbitrary points per experimental quadruplets using the Olympus CellSens imaging software program (version 2.3). Captured images of the treatment groups were compared to that of the control cells (untreated) and amongst the treatment groups to determine optimum PBM treatment.

Biochemical analysis

All biochemical assays were performed in quadruplicate and analysis was conducted 24 and 96 hpi. Results are represented relative to the control.

Table 1 Photobiomodulation parameters employed on NEBs

	Green	Near infra-red (NIR)
Light Source	Diode Laser	Diode Laser
Wavelength (nm)	525	825
Power Output (mW)	525	159
Power Density (mW/cm^2)	57.82	17.51
Emission	Continuous wave	Continuous Wave
Fluence (J/cm^2)	5 and 10	5 and 10
Time of Irradiation (s)	86 and 173	286 and 571

Proliferation ATP

Cellular proliferation of NEBs was evaluated using CellTiter-Glo® 3D ATP luminescence assay (Promega, G968A). Briefly, 100 µL volume of CellTiter-Glo® 3D reagent was added to 100 µL of NEB in media in a 96-well opaque plate. The plate was mixed for 5 min on an orbital shaker and incubated for 30 min at room temperature in the dark. Following the incubation, colorimetric changes was measured using the VICTOR Nivo® multimode plate reader, (PerkinElmer, HH35940080 EN) in relative light units (RLUs).

Live/ Dead Viability Assay

Live / dead was used to qualitatively visualise the distribution of live and dead NEB post PBM treatment. Briefly, the control and PBM treatment groups were washed thrice with ice-cold 1X PBS (200 µL). The NEBs were then suspended in 200 µL of 1X PBS followed by dual staining using 2 µL of acridine orange (AO) (1 µg/ mL) and 1 µL of ethidium homodimer-1 (EtBr) (1 µg/ mL) were added to each well and incubated for 5 min at room temperature. Following incubation NEBs were washed with 1X PBS (200 µL) and visualized using AO and EtBr channels under a Leica MICA microscope using a MICA Microhub microscope (Leica). Quantification of viability was determined by measuring the mean fluorescence intensity of each stain using ImageJ.

Lactate Dehydrogenase Assay (LDH) (Cytotoxicity)

The effects of PBM on NEBs cell membrane integrity was quantitatively assessed by detecting the quantities of cytosolic lactate dehydrogenase (LDH) produced by NEB cells with deformed membranes using the CytoTox 96® Non-Radioactive cytotoxicity assay (Promega, G179A). Briefly, 50 µL of CytoTox 96® Non-Radioactive reagent was added to equal volume of NEB media in a 96-well plate and incubated at room temperature in the dark for 10 min. VICTOR Nivo® multimode plate reader, (PerkinElmer, HH35940080 EN) was used at 490 nm absorbance.

Quantitative Polymerase Chain Reaction (qPCR)

To quantify the expression level of ADSCs marker and neuronal genes in iADSCs differentiated NEBs, qPCR was performed. Total RNA was isolated from NEBs using Quick-RNA™ MiniPrep Plus Kit (Zymo, ZR R1058), the RNA was adopted for cDNA synthesis using LunaScript RT SuperMix Kit (NEB, E3010) using universal reverse primer. Target genes Table 2 were amplified and quantified using Luna Universal qPCR Master Mix (NEB, M3003) in an Agilent Aria MX Real-Time PCR (Agilent Technologies, G8830-64001). All qPCR reactions were performed in triplicate using the following conditions:

Table 2 Primer sequence

	Forward primer (5′- 3′)	Reverse primer (5′ – 3′)
GAPDH	AGCTGAACGGGAAGCTCACT	TGCTGTAGCCAAATTCGTTG
Nestin	AGAGAGCGTAGAGGCAGTAA	GGTGCTTGAGTTTCTGGAGAT
MAP2	ACAGAGAGGGCATCTCCT ATAA	ATAGTCCCAGCCAAGGATTTG
PAX 6	GAAGGGCCAAATGGAGAAGA	TATCAGCAGTAGTTTCAGCACC
CD105	CCGCCGCACTGTGGTACATCTA	TGTGGTTGGTGCTACTGCTCT CTG
CD 44	GACAGCGTGTACCTGACTTTAT	CTCGATAAAGGGTGGGCTTATT
GFAP	GCCTCTGGATTGTGGGAATTA	GGCCTTTAGAAATGGGACAAAG

initial denaturation at 95 °C for 1 min followed by 40 cycles at 95 °C for 15 s, annealing at 60 °C for 30 s. Gene expression level was normalized to Glyceraldehyde 3-phosphate dehydrogenase (GAPDH) and the relative fold change was determined using the $2^{-(\Delta\Delta Ct)}$ method.

Immunocytochemistry of SOX-2 marker

To determine potential early transdifferentiation of immortalized ADSCs into NEBs, qualitative expression of transcription SOX-2 and Neuron-specific nuclear binding protein (Neu N) was studied using immunofluorescences. Briefly, generated NEBs were washed thrice in 1X PBS (200 µL) and fixed with 4% paraformaldehyde at room temperature for 1 h. The NEBs were washed thrice with 1X PBS (200 µL) to remove excess paraformaldehyde and permeabilized by incubation with 0.1% Triton X-100 PBS solution for 30 min at room temperature followed by washing thrice with 1X PBS (200 µL). The samples were then blocked in 10% Bovine Serum Albumin (BSA)-PBS for 1 h at room temperature. Following incubation NEBs were washed thrice with 1X PBS (200 µL) to avoid non-specific bindings and interaction. Primary (1°) and secondary (2°) antibodies were prepared according to manufacturer's protocol. Primary antibody mouse anti-SOX 2 (1:100, R&D Systems, MAB2018) and mouse anti-Neu N (1:50, Sigma-Aldrich, MAB377) was added to the NEBs and incubated for 3 h at room temperature in the dark. After 3 h incubation NEBs were washed thrice with 1X PBS (200 µL) to remove unbound primary antibodies, followed by secondary antibody staining R-phycoerythrin conjugate goat anti-mouse (1:20, Sigma Aldrich, South Africa) for 1 h at room temperature in the dark. Following secondary antibody staining, NEBs were washed with 1X PBS (200 µL) thrice followed by nuclear counter staining using 4′,6-diamidino-2-phenylindole (DAPI) solution (1 µg/ml) in PBS; and incubated for 15 min at room temperature. Lastly the NEBs were washed thrice with 1X PBS (200 µL) to remove excess DAPI and NEBs were imaged using a Leica MICA (D-35578 Wetzlar, Germany) microscope using a MICA Microhub (Leica). In addition, a negative control without primary antibody was carried out to discard non-specific binding.

Statistical analysis

All in vitro experiments were performed four times (n = 4), and experimental data are represented as means ± standard errors of the mean All in vitro acquired data were statistically analyzed using GraphPad Prism (version 10.1.1) software to determine statistical significance. Two-way analysis of variance (ANOVA) and the Turkey post hoc test was performed at a confidence interval of 0.95 to determine statistical significance between the control (untreated NEBs) and treatment groups and amongst the treatment groups. Statistical significance was set at $p < 0.05$ and was also defined as $^{*}p < 0.05$, $^{**}p < 0.01$, $^{***}p < 0.001$ and $^{****}p < 0.0001$.

Results

Morphology (Inverted light and live/dead assay)

The morphology of generated NEBs were examined using inverted light microscope using 20 X objective and data was captured 24 and 96 hpi (Fig. 2A and C).The assessment of NEB structures involved examining shape uniformity, the progression of smooth edges forming around them and the development of a bright ring as a sign of early transdifferentiation. The employment of PBM treatment towards early neural transdifferentiation is novel. Morphological analysis of the control (untreated NEBs) and the experimental groups (PBM treated) was conducted on generated NEBs with PBM treatment at 825 nm, 525 nm and the combination (825 and 525 nm). At 24 hpi the control showed the normal NEB spherical shape and when comparing to the experimental groups no distinct morphological changes was observed in the PBM treatment condition to the control.

Observation at 24 and 96 hpi revealed the emergence of smooth edges, suggesting the presence of healthy NEBs characterized by orderly cell organization [16]. The NEBs at 24 hpi maintained morphological uniformity According to morphological analysis (Fig. 2A & C), it was observed that cells that received 5 J/cm^2 and 10 J/cm^2 PBM started proliferating in a localized region, when compared to the control cells, no morphological changes were observed in cells treated with 5 J/cm^2 laser light i.e., using NIR (825 nm), G (525 nm), and the combination NIR-G (Fig. 2A). However, morphological changes i.e., formation of the necrotic core was observed in cells treated with NIR, G, and the combination of NIR and G at a light dose of 10 J/cm^2 laser. In addition, the size of the spheroids i.e., those treated with laser at light dose 5 J/cm^2 were compared to spheroids that received laser

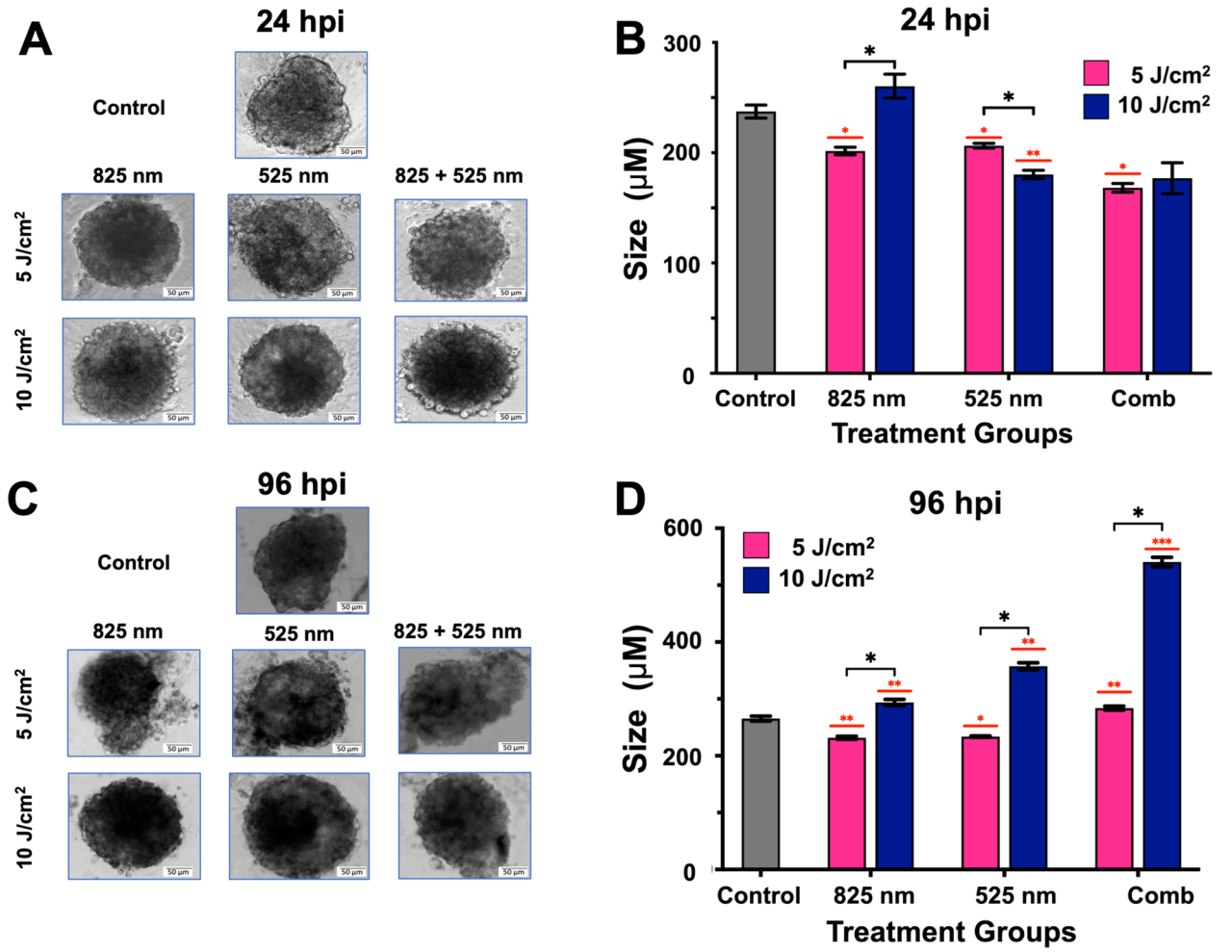

Fig. 2 Morphology and size development of neural embryoid bodies (NEBs). **A** Morphology of NEBs 24-h post-irradiation (hpi) (Magnification 20X), **B** Size development of NEBs 24 hpi, **C** Morphology of NEBs 96 hpi (Magnification 20X), **D** Size development of NEBs 96 hpi. Each bar represents the mean diameter ± standard error of the mean (SEM). Statistical significance *$p < 0.05$, ** $p < 0.01$, ***$p < 0.001$, ****$p < 0.0001$. (mean ± SEM) comparing control to the treatment groups

light irradiation at a dose of 10 J/ cm^2 (Fig. 2C). Further, significant changes in size were observed in both NIR and G experimental models 24 hpi, however, there was no significant changes in size of the combination of two laser (Fig. 2C). In another experimental model where spheroids were treated with NIR, G, and the combination of NIR with G laser light, incubated for 96 h. All treatment groups showed morphological alterations including increase in the necrotic core suggesting that cells have reached their life span and a decrease in the proliferation layer. This is seen as cells start budding of from the main spheroid in this context cells on the surface of the spheroids would tend to bud off from the original spheroid to distant part of the cell culture model in search of nutrients. Additionally, cells within the quiescent layer send cellular signals to cells in the proliferation layer (other cells) to migrate due to stress, injury lack of nutrients and oxygen exchange within the necrotic core (Fig. 2B & D).

In all experimental groups subjected to PBM treatment, a distinct brightened ring was evident, contrasting with the control group where no such ring appeared 24 hpi. The structure of NEBs was observed as spherical and compact using 5 J/cm^2 and NIR light, while minimal budding and breaking of NEBs is observed using G and NIR-G light. At a dose of 10 J/cm^2 cells maintained compact and spherical shapes. At 96 hpi using 5 J/cm^2 and all wavelengths used, there was cell shape distortion in all groups. Using 10 J/cm^2 cells maintained their spherical shape subjected to NIR and G light, while little cell shape distortion could be observed at NIR-G.

The NEB diameter is significantly influenced by the seeding density [17, 18] and optimal NEB size is

important in differentiation protocols as differentiation depends highly upon the size of the NEBs [19]. In this study, an increase in the diameter of NEBs was observed as early as 24 hpi in PBM treatment of 825 nm at fluence of 10 J/cm^2. The decrease in NEBs diameter in PBM treated groups was recorded to be significantly lower at 5 J/cm^2 in all treatment groups and maintained average size below the control. The diameter of NEBs over time at 96 hpi, increased significantly so in all PBM treated groups compared to the control at high fluences of 10 J/cm^2 with increased proliferation and growth. On the other hand NEBs following PBM treatment maintained a diameter size small than that of the control. When assessing the effects of the different fluences there is significant increase in diameter in 10 J/cm^2 compared to 5 J/cm^2.

Biochemical assays

Cytotoxicity

The release of LDH following PBM treatment was recorded, in this study at 24 hpi (Fig. 3A), there was a significant increase in cellular membrane damage at 825 nm at 5 J/cm^2 compared to the control. The amount of LDH released over time at 96 hpi (Fig. 3B), the amount of LDH released from the control decreased and a similar trend of a two-fold decrease was recorded for all PBM treatment groups at 5 J/cm^2. And an increase in LDH was recorded when treated with 525 nm and combination at 10 J/cm^2. When comparing the effects of PBM on LDH

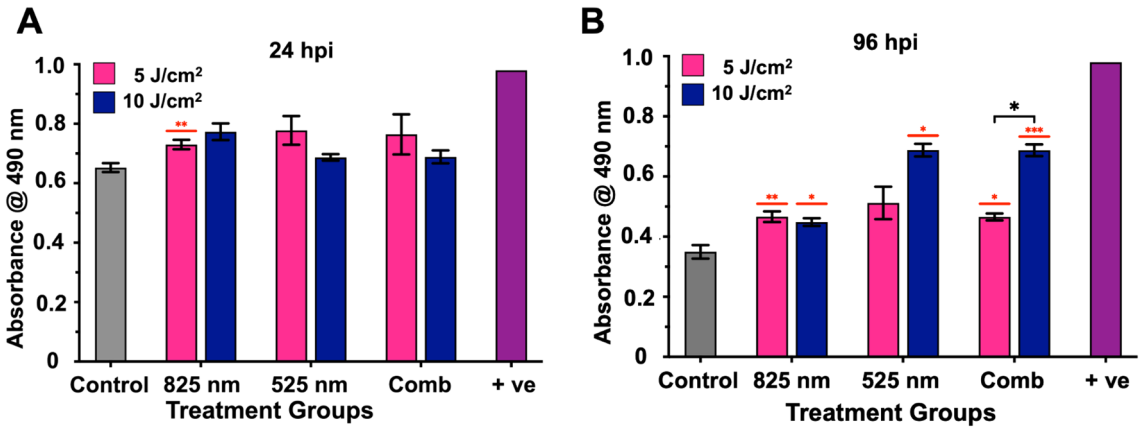

Fig. 3 LDH cytotoxicity investigating membrane integrity following PBM (**A**) 24 hpi and (**B**) 96 hpi with relation to positive control. Statistical significance *$p < 0.05$, ** $p < 0.01$, ***$p < 0.001$. (mean ± SEM) comparing control to the treatment groups. Red asterisks represent data statistical significance compared to the control and black asterisks show comparison between the groups.

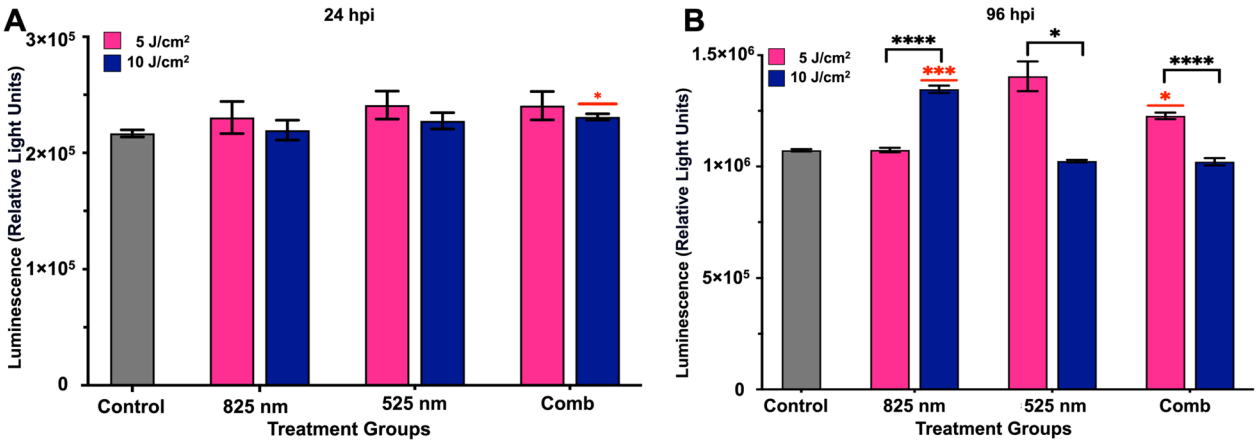

Fig. 4 ATP level evaluation following PBM treatment (**A**) 24 hpi (**B**) 96 hpi. Statistical significance *$p < 0.05$, ***$p < 0.001$ and ****$p < 0.0001$. (mean ± SEM) comparing control to the treatment groups. Red asterisks represent data statistical significance compared to the control and black asterisks show comparison between the groups

release between treatment group a significant observation was observed when comparing the combination treatment. All experimental groups had higher LDH levels than the control samples, however not to the same extent as the positive control, which is 100% toxic and causes cell death Fig. 3**.**

Proliferation In this study, intracellular ATP content within the cells was determined, as a measurement of cell proliferation and metabolic activity, following PBM treatment. Initially, following PBM at 24 hpi (Fig. 4A), experimental groups 825 nm and 525 nm maintained steady state of proliferation compared to the control with a significant increase at combination wavelength treatment at 10 J/cm^2. Over time at 96 hpi (Fig. 4B) PBM treatment at 825 nm showed significant increase compared to that of the control at 10 J/cm^2, while for the combination a significant increase in ATP metabolic activity was observed at 5 J/cm^2. When comparing amongst the treatment groups, 5 J/cm^2 showed to increase cellular metabolic activity when treated with 525 nm and the combination and at 825 nm 10 J/cm^2 showed increased metabolic activity. Indicating that PBM augments stem cell metabolic activity of time and is wavelength and fluence dependent.

Live/Dead cellular viability assay

The live/ dead assay using acridine orange and ethidium bromide (AO/ EtBr) was performed to qualitatively visualize the distribution of live and dead within the NEBs following PBM treatment. Acridine oranges dye enters live viable cells and produces green fluorescence in the nuclei while ethidium bromide only penetrates cells with damaged cytoplasmic membranes and stains the nuclei red [20, 21]. In this study we found 24 hpi (Fig. 5A and B), NEB viability remained higher compared to non-viable cells, significantly so in cells treated with 525 nm PBM at 10 J/cm^2 compared to the control. At 96 hpi (Fig. 5A and C) an increase in the amount of non-viable NEBs was observed with PBM treatment at 525 nm and the combination while other treatment groups. In this study we found that the viability of the NEBs remained above 80% throughout the study period at both 24 and 96 hpi.

A necrotic core was observed in the NEBs spheroids. The presence of the necrotic core is indictive of the insufficient nutrients and oxygen exchange within the spheroids This shows that the inner cells are not receiving adequate nutrients and oxygen [22].

Gene expression

To determine the extent to which transdifferentiation of immortalized adipose-derived stem cells (ADSCs) into neural lineage gene expression occurs, we evaluated the expression of ADSCs primary markers CD 44 (hyaluronan receptor) and CD 105 (Endoglin) and key neural markers PAX 6 (Paired-box 6), and Nestin (neuroepithelial stem cell protein) as well as the intermediate filament protein GFAP (Glial Fibrillary Acidic Protein) were evaluated **(**Fig. 6**)**. Gene expression of each gene was investigated relative to the control.

In this study, expression of CD 44 was upregulated in all treatment groups when using 5 J/cm^2 at 24 hpi (Fig. 6A), significantly so at 825 nm and 525 nm. When using 10 J/cm^2 a downregulation in expression was observed in treatment of 825 nm and 525 nm. The expression of CD44 over time, at 96 hpi (Fig. 6F) remained upregulated at 5 J/cm^2 in all treatment groups while at 10 J/cm^2 expression increased but remained low. In this study, CD 105 expression was upregulated in all treatment groups when using 10 J/cm^2 and when using 5 J/cm^2 upregulation was observed at 525 nm and the combination at 24 hpi. When comparing the different fluence it was observed that 10 J/cm^2 increased CD 105 expression at 825 nm and the combination and at 525 nm 5 J/cm^2 showed increased expression compared to the 10 J/cm^2. A significant decrease in the stem cell marker CD105 was observed over time when using 5 J/cm^2 across all wavelengths at 96 hpi. Conversely, when using 10 J/cm^2 at all wavelengths an increase in CD105 expression level is observed (Fig. 6B & G).

Results on the expression of PAX 6 indicated that at 24 hpi, there was an increase in PAX 6 expression when using 10 J/cm^2 compared to 5 J/cm^2 (Fig. 6 C). However, over time, PAX 6 expression was notable downregulated across all experimental groups. Notably, a decrease was observed particularly in groups exposed to 825 nm and the combination treatment at 10 J/cm^2 (Fig. 6 H). Overall, 10 J/cm^2 has the most impact on the down regulation of PAX 6.

In our study, early neural marker Nestin was investigated under various experimental conditions. At 5 J/cm^2 at 24 hpi (Fig. 6 D), upregulation of Nestin was observed across all experimental groups. However, at 10 J/cm^2, upregulation was noted specifically at 825 nm and in the combination group, while 525 nm showed a downregulation of the gene. Over time, there was a downregulation of Nestin expression at 825 nm and in the combination group at 5 J/cm^2. In contrast, at 10 J/cm^2 (Fig. 6I) at 96 hpi, expression levels remained higher at 825 nm and in the combination group.

The expression of intermediate filament protein glial fibrillary acidic protein (GFAP) was evaluated. At 24 hpi expression was increased at 825 nm at 10 J/cm^2 and also with the combination treatment at 5 J/cm^2. Over time the expression remained high and upregulated at 825 nm

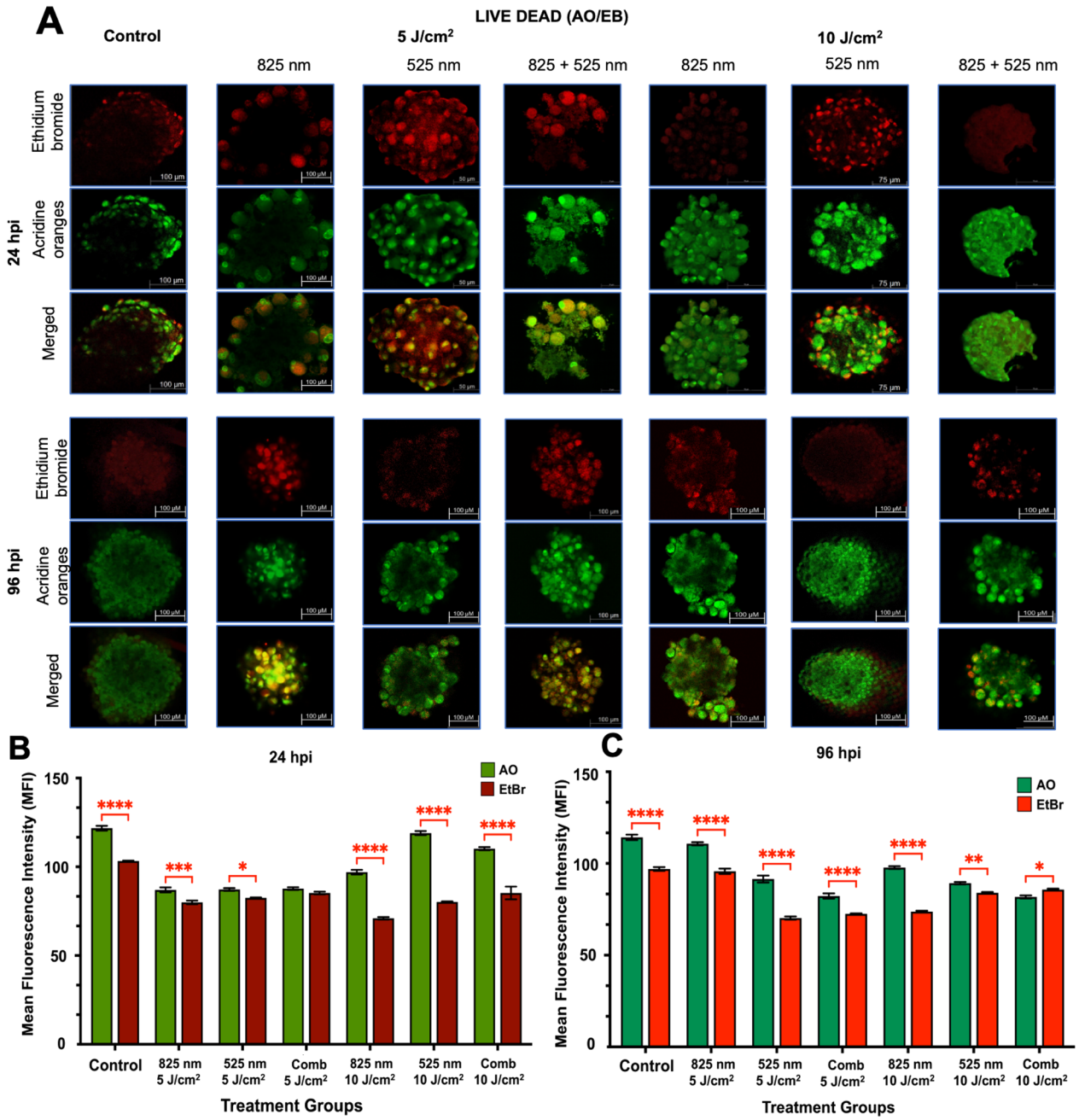

Fig. 5 Cellular viability experiment. (**A**) Live/dead assay of all samples 24 and 96 hpi. PBM treatment was conducted 24 h post seeding with NIR 825 nm, Green 525 nm and consecutive 825 and 525 nm at 5 and 10 J/cm2. Live cells appear green and dead cells appear red. (Magnification 10X) (**B**) Mean fluorescence intensity of the live/ dead assay post irradiation at 24 hpi. (**C**) Mean fluorescence intensity of the live/ dead assay post irradiation at 96 hpi. Statistical significance $*p < 0.05$, $**p < 0.01$, $***p < 0.001$, $****p < 0.0001$ (mean ± SEM comparing acridine orange (AO) and ethidium bromide (EtBr) mean fluorescence intensity)

at 10 J/cm^2 while a downregulation was observed in the combination at 5 J/cm^2. Expression at 525 nm at both time at both 5 and 10 J/cm^2 remained the same.

Immunofluorescence of SOX 2 and Neu N

Neural embryoid bodies were exposed to immunofluorescence labelling with early neural marker SRY-Box Transcription Factor 2 (SOX2) and late neural marker Neu N (Neuronal Nuclei), co-stained with DAPI to validate

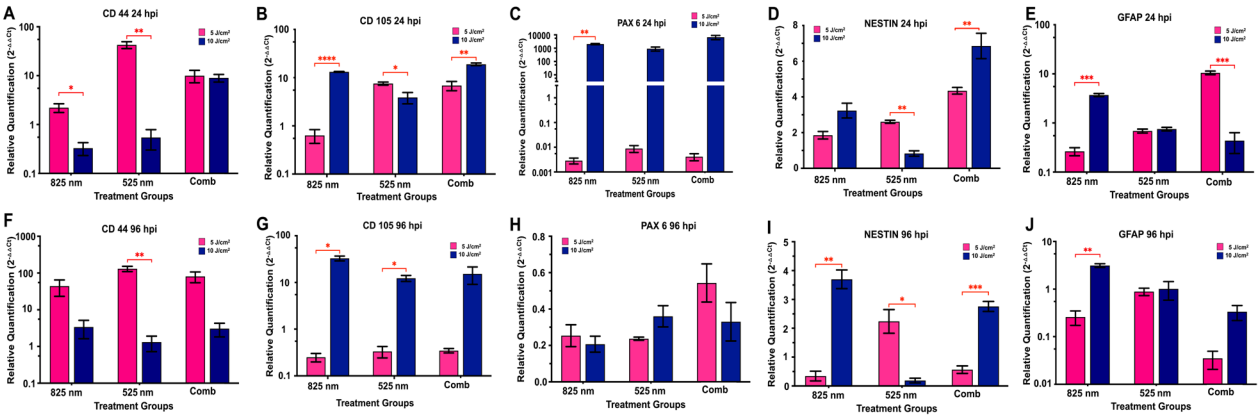

Fig. 6 The expression of ADSCs marker CD 44 and CD 105 and early neural marker PAX 6 and Nestin and glial markers GFAP. (**A**) CD 44 24 hpi, (**B**) CD 105 24 hpi, (**C**) PAX 6 (24 hpi), (**D**) NESTIN 24 hpi, (**E**) GFAP 24 hpi, (**F**) CD 44 96 hpi, (**G**) CD 105 96 hpi, (**H**) PAX 6 96 hpi,(**I**) NESTIN 96 hpi, and (**J**) GFAP 96 hpi. Statistical significance * $p < 0.05$, ** $p < 0.01$, ***$p < 0.001$, ****$p < 0.0001$. (SEM) comparing the relative expression between the treatment groups of 5 J/cm^2 and 10 J/cm^2

the neural characteristics of and visualized using a Leica MICA confocal microscope. As shown in Fig. 7A at 24 hpi, SOX2 expression was observed at 5 J/cm^2 across all treatment groups, with notably higher expression at 825 nm and in the combination group compared to the control, which exhibited no detectable expression. At 24 hpi expression is observed at 5 J/cm^2 in all treatment groups more so when using 825 nm and the combination compared to the control where no expression is exhibited. Over time the expression of SOX 2 at 5 J/cm^2 tapering down of SOX 2 expression was observed at 96 hpi.

The expression of neuronal nuclei marker (NeuN) (Fig. 7B) was assessed in all treatment groups, at both 5 J/cm^2 and 10 J/cm^2. Intially at 24 hpi, NeuN expression was observed in the control group and all treatment groups at 5 J/cm^2. In contrast, no expression was detected at 10 J/cm^2 in any of the groups. Over time, NeuN expression in the 5 J/cm^2 groups decreased across all treatment conditions (825 nm, 525 nm, and combination), while in the 10 J/cm^2 groups, NeuN expression became progressively more evident. A similar decreasing trend in expression was noted in the control group over time. To validate these findings, a negative control (Fig. 7) for immunofluorescence was performed, and no signal was detected, confirming the specificity of SOX 2 and NeuN expression in the experimental groups.

Discussion

Adipose-derived stem cells have gained prominence in the field of regenerative medicine during the last decade. ADSCs appear to be the most beneficial cell type for regenerative treatments because of their simple accessibility and multipotency [23]. One of the major challenges in stem cell-based therapies is the translation of ADSCs-based therapies (*in* vitro) to clinical practice (in vivo) [23]. Huang et al. (2022) have underscored the potential of 3D culture environments to enhance cellular proliferation and differentiation [24]. Moreover, the application of PBM in 3D cell culture environment presents an intriguing avenue for investigating the effects on stem cell trans differentiation.

Herein, we characterized NEBs derived from ADSCs and assessed their morphology, viability, metabolic activity, and differentiation following PBM. PBM results are highly dependent on the parameters, including fluence (J/cm^2), exposure time (sec), and number of irradiation treatments applied [25].

Nie et al. (2023) elucidated a biphasic dose–response to PBM, suggesting that NEBs may not be significantly affected by laser fluence and wavelength in a 2D environment [26]. This response in a 3D cell culture context remains unvalidated. NEBs typically exhibit three layers: the necrotic core, quiescent layer, and proliferative layer. These layers indicate differentiation status and overall cell health, with the necrotic core arising from inadequate nutrients, the quiescent layer showing reduced metabolic activity, and the proliferative layer displaying active cell division. PBM at 825 nm and 10 J/cm^2 notably enhanced NEB size, indicative of increased cellular proliferation and reduced cytotoxicity. The observed expansion aligns with previous findings that PBM promotes cellular growth and tissue repair through improved mitochondrial function and reduced oxidative stress [27, 28].

Wavelength-specific effects are also notable. At 825 nm, 10 J/cm^2 significantly improves cell viability and proliferation, accompanied by decreased lactate dehydrogenase (LDH) levels, indicating reduced cellular damage. This is in line with findings that longer wavelengths

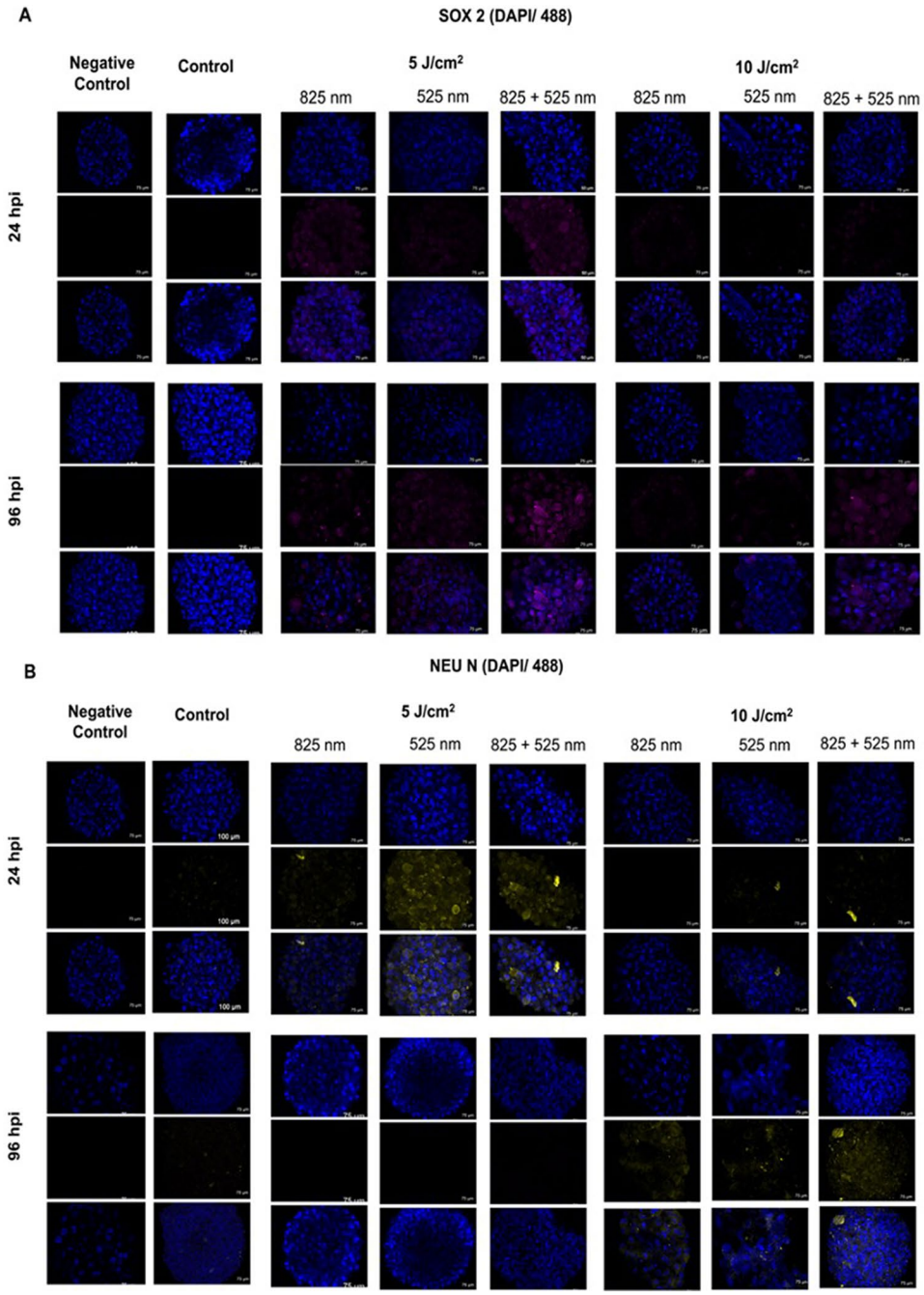

Fig. 7 Immunofluorescence staining against SOX 2 and Neu N at 5 and 10 J/cm^2 24 and 96 hpi. Nuclei stained with DAPI and internal markers (**A**) SOX 2 stained with pink and (**B**) Neu N stained with yellow. Objective of 10 X

(near-infrared) are often associated with enhanced cellular health and proliferation, likely due to better tissue penetration and reduced cellular toxicity [29, 30]. Conversely, 525 nm and combined treatments at 10 J/cm^2 are less effective in maintaining these parameters, suggesting that shorter wavelengths might not support cell viability and proliferation as effectively at higher doses.

In the process differentiation, expression of ADSCs markers is expected to decrease while neural markers are expected to increase. The ADSC marker CD44, a cell surface glycoprotein expressed by various immune and progenitor cells was investigated [31]. In this study expression of CD 44 remained upregulated at 5 J/cm2 in all treatment group at both 24 and 96 hpi. CD44 has

been found to be expressed in certain populations of neural progenitors during neurogenesis. Although it is traditionally associated with mesenchymal stem cells, its expression in neural progenitors could indicate its involvement in maintaining stemness and the regulation of the progenitor state during early neural differentiation [32]. During early stages of differentiation, CD44 may still be expressed as ADSCs transition into neural progenitors, as observed with 5 J/cm^2. As cells further more specialize neural lineage (e.g. neurons or glia), CD44 expression may decrease or be maintained at lower levels in some populations[33], coinciding with higher doses of 10 J/cm^2.

CD105, also known as endoglin, is a marker for endothelial cells and mesenchymal stem cells, and its expression can vary based on the cellular microenvironment and differentiation stage [34]. Unexpectedly, ADSCs marker CD105 expression was overall upregulated significantly at 10 J/cm^2 over time instead of decreasing. which might be attributed to the heterogeneous cell population within the NEBs. The mixed cellular composition could lead to variations in CD105 expression levels, influencing the observed data. Previous research by Wen and colleagues they showed that large spheroids actively proliferation are likely to be heterogenous [35]. This is because cells in the outer region are actively proliferating, whereas those in the inner region are quiescent due to restricted nutrient and gas exchange [36].

In contrast, Pax6 expression, a key transcription factor in neural development [37], did not show consistent expression across treatment groups but exhibited an early spike at 10 J/cm^2 followed by a decrease. This pattern may reflect a transient activation of neural progenitor pathways, with subsequent downregulation as cells advance through differentiation stages or due to the complex interplay of PBM with cellular signalling pathways [38, 39]. Nestin is a widely recognized intermediate filament protein commonly used as a marker for neural precursor cells [40]. In our study, the increased expression of Nestin in NEBs treated with PBM at 825 nm and 10 J/cm^2 confirms the promotion of neural precursor cell populations. This finding aligns with the established role of Nestin as an indicator of neural progenitors, which are capable of further differentiation into mature neurons and glia [41].

GFAP (Glial Fibrillary Acidic Protein) encodes the key intermediate filament protein. GFAP is a marker commonly associated with astrocytes in the central nervous system [42]. When adipose-derived mesenchymal stem cells are differentiated into neural lineages, temporal changes in GFAP expression may be observed, reflecting stages of neural differentiation[43]. In a previous study, it was found that there were small increases in GFAP following differentiation treatment compared to the non-differentiated ADSCs. The results revealed minor changes in the study time frame [43]. However, even low levels of GFAP expression in these mesenchymal ADSCs suggest an early stage of neural differentiation, potentially indicating a shift towards a more glial lineage [43, 44]. In this study, early expression of GFAP was observed in cells treated with PBM at 10 J/cm^2 and 825 nm consistently over time suggesting early differentiation. This slight upregulation may indicate the cells are committing to a neural fate, but still maintain some stemness.

SOX 2 is a well-established pluripotent transcription factor that plays an essential role in establishing and maintaining pluripotent [45]. SOX 2 has been reported to be involved in embryogenesis proliferation and maintains of stem cell germ cells [46]. At 5 J/cm^2, SOX 2, is expressed across all wavelengths (825 nm, 525 nm, and their combination). However, SOX 2 expression is sensitive to environmental conditions conducive to stem cell maintenance for SOX 2 expression. This observation aligns with reports suggesting that excessive stress or oxidative conditions can downregulate stem cell markers [47].

Neuronal nuclei (NeuN) is a neuron-specific nuclear protein that serves as a reliable marker for identifying mature neurons in various regions of the brain [48]. At 5 J/cm^2, NeuN expression was robust across all wavelengths at the early stages, but diminished over time, suggesting that lower energy densities may be effective for initiating neuronal differentiation but are insufficient for long-term maintenance. This observation aligns with the understanding that Neu N is expressed in differentiating and terminally differentiated neurons throughout ontogeny, which suggests that while initial differentiation may be supported, sustaining these effects may require additional stimulation [48]. Conversely, the delayed yet progressive increase in Neu N expression at 10 J/cm^2 at 96 hpi suggests that higher energy densities may require more time to elicit a cellular response but can potentially promote sustained neuronal differentiation. This results are consistent with previous studies suggesting that near-infrared light can modulate glial activity by promoting cellular repair mechanisms and reducing oxidative stress [2]. Studies have shown that higher PBM doses can activate cellular signalling pathways that enhance neuronal differentiation and survival, albeit in a delayed manner [49].

Conclusion

This study demonstrates that PBM using wavelengths of 525 nm, 825 nm, and their combination effectively influences neural differentiation in NEBs derived from iADSCs. Lower doses of PBM (5 J/cm^2) support the maintenance of pluripotency, as indicated by the expression of SOX2 and Neu N at 24 hpi. In contrast, higher

doses (10 J/cm^2) at 825 nm improve cellular health and proliferation, likely due to enhanced tissue penetration and reduced cellular toxicity. However, these higher doses may also induce differentiation or stress, leading to altered marker expression. The observed variability in cellular populations and marker responses underscores the need for more refined methods to accurately assess PBM effects. Employing advanced analytical techniques and three-dimensional in vitro models could further elucidate PBM's role in stem cell differentiation and optimize protocols for neural tissue engineering.

Future directions

A more comprehensive assessment of NEB differentiation potential would provide significant insights into their utility in regenerative medicine. Future studies should include differentiation assays to assess the potential of NEBs to differentiate into specific neuronal subtypes or other cell lineages. Molecular characterization to evaluate the expression of key markers associated with neuronal differentiation and maturation and investigating the functional properties of NEBs, such as their response to stimuli and their ability to form neural networks.

This study has several notable limitations that complicate the interpretation of PBM effects. Specifically, the lack of SOX2 detection at higher doses (10 J/cm^2) and the transient nature of Pax6 expression introduce uncertainty about the dose-dependent effects of PBM, potentially indicating that high doses may induce cellular stress or accelerate differentiation processes. Furthermore, the variation in NeuN expression at 5 J/cm^2 and 10 J/cm^2 at the different time points could indicate a non-linear dose–response relationship. It might be useful to conduct additional experiments with intermediate doses to better understand the dose–response curve. These issues highlight the need for further investigation into how different PBM doses affect cellular outcomes. Future studies should also implement and develop 3D in vitro models to provide an accurate assessment of PBM effects and improve the optimization of differentiation protocols for ADSC-derived NEBs, as two-dimensional models doesn't capture the complex in vivo environment.

Acknowledgments
The authors would like to acknowledge the university of Johannesburg for their facilities and the National Laser Centre for their laser equipment used in this study. We acknowledge Promolab Pty Ltd T/A Separations for their partnership with the Laser Research Centre, providing the Leica Mica Microhub in support of the microscopy image featured in this publication.

Author contributions
PM, AC—Conceptualization; PM and AC—Writing—Original Draft; PM, HA and AC—Writing—Review & Editing; PM—Visualization; AC and HA—Supervision; AC and HA—Funding acquisition. All authors read and approved the final manuscript.

Funding
This research was funded by the National Research Foundation of South Africa Thuthuka Instrument, grant number TTK2205035996; the Department of Science and Innovation (DSI) funded African Laser Centre (ALC), grant number HLHA23X task ALC-R007; the University Research Council, grant number 2022URC00513; the National Research Foundation Doctoral grant, grant number PMDS22070532778; and the Department of Science and Innovation South African Research Chairs Initiative (DSI-NRF/SARChI), grant number 98337.

Availability of data and materials
The raw and analysed data used to support the findings of this study are available from the corresponding author upon request.

Declarations

Ethics approval and consent to participate
(1) Title of the approved project: Differentiation of ADMSCS into brain organoids using photobiomodulation for developmental and disease modeling and regeneration; (2) Name of the institutional approval committee or unit: University of Johannesburg Faculty of Health Sciences Research Ethics Committee; (3) Approval number: REC-1972–2023 (4) Date of approval: 21 April 2023.

Consent for publication
NA.

Competing interests
The authors declare that the research was conducted in the absence of any commercial or financial relationships that could be construed as a potential conflict of interest.

Author details
[1]Laser Research Centre, Faculty of Health Sciences, University of Johannesburg, P.O. Box 17011, Doornfontein 2028, South Africa.

Received: 28 March 2024 Accepted: 3 December 2024
Published online: 20 December 2024

References

1. Mahla RS. Stem Cells Applications in Regenerative Medicine and Disease Therapeutics. Int J Cell Biol [Internet]. 2016 [cited 2023 Dec 22];2016:1–24. Available from: /pmc/articles/PMC4969512/
2. George S, Hamblin MR, Abrahamse H. Neuronal differentiation potential of primary and immortalized adipose stem cells by photobiomodulation. J Photochem Photobiol B. 2022;230: 112445.
3. Jansen Van Rensburg M, Crous A, Abrahamse H. Promoting Immortalized Adipose-Derived Stem Cell Transdifferentiation and Proliferation into Neuronal-Like Cells through Consecutive 525 nm and 825 nm Photobiomodulation. Stem Cells Int. 2022;2022:1–15.
4. Iacomi DM, Rosca AM, Tutuianu R, Neagu TP, Pruna V, Simionescu M, et al. Generation of an Immortalized Human Adipose-Derived Mesenchymal Stromal Cell Line Suitable for Wound Healing Therapy. Int J Mol Sci [Internet]. 2022 [cited 2024 Feb 12];23:1–19. Available from: https://pubmed.ncbi.nlm.nih.gov/36012192/
5. Poliwoda S, Noor N, Downs E, Schaaf A, Cantwell A, Ganti L, et al. Stem cells: a comprehensive review of origins and emerging clinical roles in medical practice. Orthop Rev (Pavia) [Internet]. 2022 [cited 2024 Aug 1];14:1–9. Available from: https://doi.org/10.52965/001c.37498
6. Lopez A, Brundage C. Wound Photobiomodulation Treatment Outcomes in Animal Models. J Vet Med. 2019;2019:1–9.
7. Chang SY, Lee MY. Photobiomodulation of Neurogenesis through the Enhancement of Stem Cell and Neural Progenitor Differentiation in the Central and Peripheral Nervous Systems. Int J Mol Sci [Internet]. 2023 [cited 2024 Feb 12];24:1–16. Available from: /pmc/articles/PMC10607539/
8. Pan LC, Hang NLT, Colley MMS, Chang J, Hsiao YC, Lu LS, et al. Single Cell Effects of Photobiomodulation on Mitochondrial Membrane Potential and Reactive Oxygen Species Production in Human Adipose

Mesenchymal Stem Cells. Cells [Internet]. 2022 [cited 2024 Jan 13];11:987. Available from: https://www.mdpi.com/2073-4409/11/6/972/htm
9. Dompe C, Moncrieff L, Matys J, Grzech-Le K, Kocherova I, Bryja A, et al. Photobiomodulation-Underlying Mechanism and Clinical Applications. J Clin Med [Internet]. 2020 [cited 2023 Mar 6];9:1–17. Available from: www.mdpi.com/journal/jcm
10. Ahrabi B, Tavirani MR, Khoramgah MS, Noroozian M, Darabi S, Khoshsirat S, et al. The Effect of Photobiomodulation Therapy on the Differentiation, Proliferation, and Migration of the Mesenchymal Stem Cell: A Review. J Lasers Med Sci [Internet]. 2019;10:S103
11 Van Rensburg MJ, Crous A, Abrahamse H. Potential of photobiomodulation to induce differentiation of adipose- derived mesenchymal stem cells into neural cells. Curr Stem Cell Res Ther. 2021;16:307–22.
12. Luo L, Hu DH, Yin JQ, Xu RX. Molecular mechanisms of transdifferentiation of adipose-derived stem cells into neural cells: Current status and perspectives. Stem Cells Int. Hindawi Limited 2018;1–14.
13. Radhakrishnan S, Trentz OA, Reddy MS, Rela M, Kandasamy M, Sellathamby S. In vitro transdifferentiation of human adipose tissue-derived stem cells to neural lineage cells - a stage-specific incidence. Adipocyte. 2019;8:177.
14 Kim MS, Kim DH, Kang HK, Kook MG, Choi SW, Kang KS. Modeling of hypoxic brain injury through 3d human neural organoids. Cells. 2021;10:1–17.
15. Azmi N, Mustaffa Al Bakri SS, Khor W, Hamzah SN, Ferdaos N, Ling KH, et al. Neural fate commitment of rat full-term amniotic fluid stem cells via three-dimensional embryoid bodies and neurospheres formation. IBRO Neurosci Rep. 2023;14:235–43.
16. Lancaster MA, Knoblich JA. Generation of cerebral organoids from human pluripotent stem cells. Nat Protoc. 2014;9:2329–40.
17. Aguilar Cosme JR, Gagui DC, Green NH, Bryant HE, Claeyssens F. In vitro low-fluence photodynamic therapy parameter screening using 3D tumor spheroids shows that fractionated light treatments enhance phototoxicity. ACS Biomater Sci Eng. 2021;7:5078–89.
18. Son B, Kim JA, Cho S, Jeong GJ, Kim BS, Hwang NS, et al. Lineage specific differentiation of magnetic nanoparticle-based size controlled human embryoid body. ACS Biomater Sci Eng. 2017;3:1719–29. https://doi.org/10.1021/acsbiomaterials.7b00141.
19. Mohr JC, Zhang J, Azarin SM, Soerens AG, de Pablo JJ, Thomson JA, et al. The microwell control of embryoid body size in order to regulate cardiac differentiation of human embryonic stem cells. Biomaterials. 2010;31:1885–93.
20. Georgieva A, Todorova K, Iliev I, Dilcheva V, Vladov I, Petkova S, et al. Hemocyanins from helix and rapana snails exhibit in vitro antitumor effects in human colorectal adenocarcinoma. Biomedicines. 2020;8:208.
21. Salehi F, Behboudi H, Kavoosi G, Ardestani SK. Monitoring ZEO apoptotic potential in 2D and 3D cell cultures and associated spectroscopic evidence on mode of interaction with DNA. Sci Rep. 2017;7:1–14.
22 Barisam M, Saidi MS, Kashaninejad N, Nguyen NT. Prediction of necrotic core and hypoxic zone of multicellular spheroids in a microbioreactor with a U-shaped barrier. Micromachines (Basel). 2018;9:1–19.
23. Qin Y, Ge G, Yang P, Wang L, Qiao Y, Pan G, et al. An update on adipose-derived stem cells for regenerative medicine: where challenge meets opportunity. Adv Sci. 2023;10:1–27. https://doi.org/10.1002/advs.202207334.
24. Huang X, Huang Z, Gao W, Gao W, He R, Li Y, et al. Current advances in 3D dynamic cell culture systems. Gels. 2022;8:829–49.
25. Mokoena D, Dhilip Kumar SS, Houreld NN, Abrahamse H. Role of photobiomodulation on the activation of the Smad pathway via TGF-β in wound healing. J Photochem Photobiol. 2018;189:138–44.
26. Nie F, Hao S, Ji Y, Zhang Y, Sun H, Will M, et al. Biphasic dose response in the anti-inflammation experiment of PBM. Lasers Med Sci. 2023;38:1–14.
27 Salehpour F, Mahmoudi J, Kamari F, Sadigh-Eteghad S, Rasta SH, Hamblin MR. Brain photobiomodulation therapy: a narrative review. Mol Neurobiol. 2018;55:6601–36. https://doi.org/10.1007/s12035-017-0852-4.
28. Tripodi N, Sidiroglou F, Fraser S, Husaric M, Kiatos D, Apostolopoulos V, et al. The effects of polarized photobiomodulation on cellular viability, proliferation, mitochondrial membrane potential and apoptosis in human fibroblasts: Potential applications to wound healing. J Photochem Photobiol. 2022;236:1–8.
29. Wang Y, Huang YY, Wang Y, Lyu P, Hamblin MR. Red (660 nm) or near-infrared (810 nm) photobiomodulation stimulates, while blue (415 nm), green (540 nm) light inhibits proliferation in human adipose-derived stem cells. Sci Rep. 2017;7:1–10.
30 De Freitas LF, Hamblin MR. Proposed mechanisms of photobiomodulation or low-level light therapy. IEEE J Sel Top Quant Elect. 2017;22:348–64.
31. Mildmay-White A, Khan W. Cell surface markers on adipose-derived stem cells: a systematic review. Curr Stem Cell Res Ther. 2017;12:484–92.
32. Okolicsanyi RK, Camilleri ET, Oikari LE, Yu C, Cool SM, Van Wijnen AJ, et al. Human mesenchymal stem cells retain multilineage differentiation capacity including neural marker expression after extended in vitro expansion. PLoS One. 2015;10:1–29.
33. Su W, Foster SC, Xing R, Feistel K, Olsen RHJ, Acevedo SF, et al. CD44 transmembrane receptor and hyaluronan regulate adult hippocampal neural stem cell quiescence and differentiation. J Biol Chem. 2017;292:4445.
34 Ponnaiyan D, Jegadeesan V. Comparison of phenotype and differentiation marker gene expression profiles in human dental pulp and bone marrow mesenchymal stem cells. Eur J Dent. 2014;8:313.
35. Wen Z, Liao Q, Hu Y, You L, Zhou L, Zhao Y. A spheroid-based 3-D culture model for pancreatic cancer drug testing, using the acid phosphatase assay. Brazil J Med Biol Res. 2013;46:634–42.
36. Edmondson R, Broglie JJ, Adcock AF, Yang L. Three-dimensional cell culture systems and their applications in drug discovery and cell-based biosensors. Assay Drug Dev Technol. 2014;12:218.
37 Mishra S, Maurya SK, Srivastava K, Shukla S, Mishra R. Pax6 influences expression patterns of genes involved in neuro- degeneration. Ann Neurosci. 2015;22:231.
38 Ahrabi B, Tavirani MR, Khoramgah MS, Noroozian M, Darabi S, Khoshsirat S, et al. The effect of photobiomodulation therapy on the differentiation, proliferation, and migration of the mesenchymal stem cell: a review. J Lasers Med Sci. 2019;10:s103.
39 Shohayeb B, Cooper HM. The ups and downs of Pax6 in neural stem cells. J Biol Chem. 2023;299:1–3.
40 Bernal A, Arranz L. Nestin-expressing progenitor cells: function, identity and therapeutic implications. Cell Mol Life Sci. 2018;75:2195.
41. Wang Z, Zheng Y, Zheng M, Zhong J, Ma F, Zhou B, et al. Neurogenic niche conversion strategy induces migration and functional neuronal differentiation of neural precursor cells following brain injury. Stem Cells Dev. 2020;29:235–48.
42. Hol EM, Pekny M. Glial fibrillary acidic protein (GFAP) and the astrocyte intermediate filament system in diseases of the central nervous system. Curr Opin Cell Biol. 2015;32:121–30.
43. Pelegri NG, Milthorpe BK, Gorrie CA, Santos J. Neurogenic marker expression in differentiating human adipose derived adult mesenchymal stem cells. Stem Cell Investig. 2023;10:1–15.
44. Safford KM, Hicok KC, Safford SD, Halvorsen YDC, Wilkison WO, Gimble JM, et al. Neurogenic differentiation of murine and human adipose-derived stromal cells. Biochem Biophys Res Commun. 2002;294:371–9.
45 Zhang S, Bell E, Zhi H, Brown S, Imran SAM, Azuara V, et al. OCT4 and PAX6 determine the dual function of SOX2 in human ESCs as a key pluripotent or neural factor. Stem Cell Res Ther. 2019;10:1–14.
46. Wei L, Wang L, Pan J, Liu L, Wang P, Wei J, Xiaoming X, Xing Q, Liu P, Wende W, Li G, Zheng X. Specificity and application of SOX2 antibody. Poultry Sci. 2020;99(5):2385–94. https://doi.org/10.1016/j.psj.2020.01.001.
47. Chang S-Y, Lee MY. Photobiomodulation of neurogenesis through the enhancement of stem cell and neural progenitor differentiation in the central and peripheral nervous systems. Int J Mol Sci. 2023;24(20):15427. https://doi.org/10.3390/ijms242015427.
48 Guselnikova VV, Korzhevskiy DE. NeuN as a neuronal nuclear antigen and neuron differentiation marker. Acta Naturae. 2015;7(2):42–7. https://doi.org/10.32607/20758251-2015-7-2-42-47.
49. Ma Y, Li P, Ju C, Zuo X, Li X, Ding T, et al. Photobiomodulation attenuates neurotoxic polarization of macrophages by inhibiting the notch1-HIF-1α/NF-κB signalling pathway in mice with spinal cord Injury. Front Immunol. 2022;13:1–6.

Publisher's Note